INTERNATIONAL JOURNAL OF CLIMATOLOGY
Int. J. Climatol. **28**: 881–892 (2008)
Published online 1 August 2007 in Wiley InterScience
(www.interscience.wiley.com) DOI: 10.1002/joc.1589

RMetS
ROYAL METEOROLOGICAL SOCIETY

Mass balance of a slope glacier on Kilimanjaro and its sensitivity to climate

Thomas Mölg,[a]* Nicolas J. Cullen,[b] Douglas R. Hardy,[c] G. Kaser[a] and L. Klok[d]

[a] *Tropical Glaciology Group, Department of Earth and Atmospheric Sciences, University of Innsbruck, Innrain 52, 6020 Innsbruck, Austria*
[b] *Department of Geography, University of Otago, PO Box 56, Dunedin 9054, New Zealand*
[c] *Climate System Research Center, Department of Geosciences, University of Massachusetts, 611 North Pleasant Street, Amherst, MA 01003-9297, USA*
[d] *Royal Dutch Meteorological Institute, Postbus 201, 3730 AE De Bilt, Netherlands*

ABSTRACT: Meteorological and glaciological measurements obtained at 5873 m a.s.l. on Kersten Glacier, a slope glacier on the southern flanks of Kilimanjaro, are used to run a physically-based mass balance model for the period February 2005 to January 2006. This shows that net shortwave radiation is the most variable energy flux at the glacier-atmosphere interface, governed by surface albedo. The majority of the mass loss (∼65%) is due to sublimation (direct conversion of snow/ice to water vapour), with melting of secondary importance. Sensitivity experiments reveal that glacier mass balance is 2–4 times more sensitive to a 20% precipitation change than to a 1 °C air temperature change. These figures also hold when the model is run with input data representative of a longer term (1979–2004) mean period. Results suggest that a regional-scale moisture projection for the 21st century is crucial to a physically-based prediction of glacier retention on Africa's highest mountain. Copyright © 2007 Royal Meteorological Society

KEY WORDS glaciers and climate; mass balance modelling; tropical glaciers

Received 5 December 2006; Revised 30 May 2007; Accepted 3 June 2007

1. Introduction

As a part of the East African rift valley system, the Kilimanjaro massif stands at the Kenya-Tanzania border (3°04′S/37°21′E) ∼300 km from the Indian Ocean coastline. The massif consists of three peaks: Shira, Mawenzi, and Kibo. The latter harbours the highest point in Africa (Uhuru Peak, 5895 m a.s.l.), and is the only one to retain glaciers. The 2003 glacier surface area estimate is 2.51 km^2 (Cullen *et al*., 2006) (Figure 1), compared to ∼20 km^2 around 1880 when the ongoing recession started (Osmaston, 1989). Proxy evidence for the longer term past (ice cores: Thompson *et al*., 2002) and recent past (circulation patterns: Hastenrath, 2001; Mölg *et al*., 2006) suggests that glacier evolution on Kilimanjaro mainly reflects regional dry and humid periods in Africa. To extend these findings to the present-day, we focus here on the sensitivity of the glaciers to present climate (i.e. the most recent years and decades). Owing to an expanded network of meteorological and glaciological measurements on Kibo in 2005 (Section 2), a high-resolution physical model can be used for the first time to precisely quantify the most direct link between atmospheric forcing and glacier volume response: the mass balance of the glacier.

Over the 20th century, tropical glaciers worldwide have shown a strong sensitivity to atmospheric moisture (precipitation and thus surface albedo, air humidity, cloudiness and thus solar radiation) in addition to air temperature (Kaser and Osmaston, 2002). This finding is based on studies in the South American Andes (e.g. Kaser and Georges, 1997; Wagnon *et al*., 2001; Francou *et al*., 2003; Kaser *et al*., 2003; Favier *et al*., 2005) as well as in Equatorial East Africa (Kruss and Hastenrath, 1987; Kaser and Osmaston, 2002; Mölg *et al*., 2003a; Mölg and Hardy, 2004). Regarding the large-scale forcing of the local glacier-climate interaction, evidence is increasing that sea surface temperatures and associated circulation modes control moisture availability on tropical high mountains, and thus mass balance fluctuations and shifts (Francou *et al*., 2003; Mölg *et al*., 2006). The importance of atmospheric moisture for present glacier mass balance has also been demonstrated on Kilimanjaro by intensified research over the last few years (e.g. Mölg and Hardy, 2004; Cullen *et al*., 2006; Section 2). Still, different glacier systems exist on Kilimanjaro (see below), and the mass balance-climate link of a sloping glacier surface has not yet been examined in detail. Section 2 provides a review of the glacier systems, while the available data and the model employed are described in Section 3. Section 4 presents the results and a discussion of the findings.

* Correspondence to: Thomas Mölg, Department of Earth and Atmospheric Sciences, University of Innsbruck, Innrain 52, 6020 Innsbruck, Austria. E-mail: thomas.moelg@uibk.ac.at

2. Climate and glacier systems on Kilimanjaro

Climate in East Africa and the Kilimanjaro region is governed by a bimodal distribution of precipitation, with the 'long rains' from March to May (MAM) and the 'short rains' from October to December (OND) (e.g. Hastenrath, 2001). A short dry season in January/February (JF) and a core dry season from June to September (JJAS) separate the wet seasons. Long-term meteorological records in East Africa are confined to lower elevations (Rodhe and Virji, 1976), but the observed glacier recession on Kilimanjaro from the late 19th century to the present provides an opportunity to derive long-term climate change at high elevations (mid troposphere) if the present glacier-climate interaction is understood. To take advantage of this opportunity, three automatic weather stations (AWSs) were installed on Kibo's summit area (>5700 m a.s.l.) (Figure 1). AWS1 has been running since February 2000 on the flat surface of the Northern Icefield and is designed for long-term monitoring of the high-altitude climate. The other stations have been in operation since February 2005. AWS2 addresses the special case of vertical ice walls on the summit plateau (Figure 1) (Mölg *et al*., 2003b), and AWS3 is explicitly designed to run models of the glacier-climate interaction. This station is located at 5873 m a.s.l. in the upper region of the sloping Kersten Glacier (a part of the Southern Icefield) and provides the main data source for the present study (Section 3.1). Local slope and aspect at AWS3 are 18° and 200° (from north), respectively.

Kilimanjaro is peculiar amongst glacierized tropical mountains, as there are different glacier types that respond differently to climatic forcing (Kaser *et al*., 2004). Clustering them into two glacier systems, Cullen *et al*. (2006) show that (1) slope glaciers (<5700 m a.s.l., Figure 1) have retreated more slowly in recent decades than in the early 20th century, while (2) the tabular-shaped plateau glaciers on Kibo's almost flat summit plateau (≥5700 m a.s.l., Figure 1) show a more constant area loss over the entire century. Although the 5700 m–contour delineates these two systems well, the situation is slightly different in the southern sector where – owing to the existence of the ridge harbouring Uhuru Peak (Figure 1) – sloping glaciers start above 5700 m a.s.l. (*cf* altitude and local slope of AWS3 as given above). The distribution of slope glaciers on Kibo has been asymmetric not just at present but in the recent and longer term past as well (Osmaston, 1989), with the largest ones in the southern sector (Figure 1). In terms of glacier surface area, slope glaciers presently contribute ∼50% to total glacierization on Kilimanjaro while they were persistently greater than plateau glaciers in the past century (Cullen *et al*., 2006). The constant areal loss of plateau glaciers is due to solar radiation-maintained recession of the vertical ice walls (Figure 1) which, once established, lead to an irreversible retreat of the glaciers they margin (Mölg *et al*., 2003b). Thus, plateau glaciers have two physically distinctive features that have been referred to as glacier regimes (Kaser *et al*., 2004): their horizontal glacier surfaces (HGSs), and the vertical ice walls at their margin. Mass gain over many consecutive years on the HGSs (and associated perennial snow cover and glacier build-up on the presently ice-free areas of the summit plateau) seems necessary to prevent formation of vertical ice walls, and hence the constant retreat of plateau glaciers. Mölg and Hardy (2004) investigated 19 months of mass balance (during 2001–2002) of such a HGS on the Northern Icefield (at AWS1) with an energy balance model. They showed that HGSs on Kibo are extremely sensitive to precipitation but much less so to air temperature variability, which leaves precipitation as the most important variable for mass balance on the HGSs. The present study complements this work for the sloping glacier surfaces on Kibo. The extension of measurements in 2005 (described above) along with an upgraded model (Section 3.2) allow inclusion of greater details in the modelling this time.

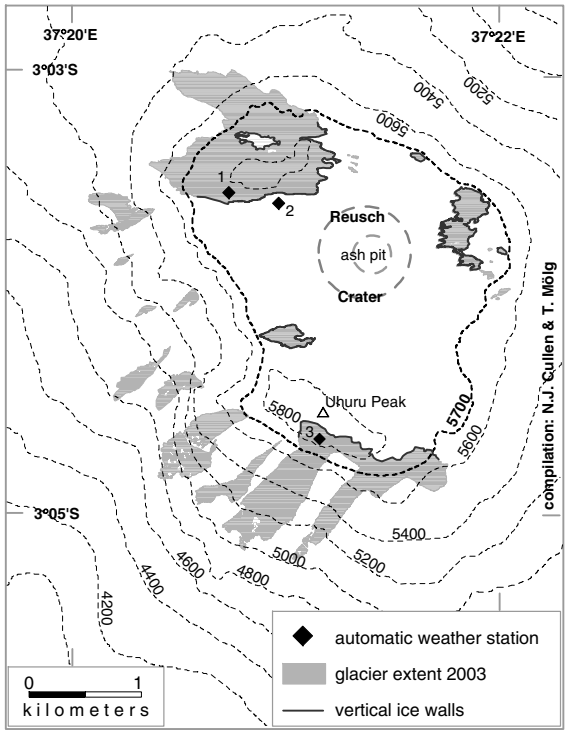

Figure 1. Glacier extent on Kibo in 2003 (Cullen *et al*., 2006). The location of automatic weather stations and vertical ice walls are also shown (UTM zone 37 S projection, contours are in metres, equidistance 200 m). The highlighted 5700 m contour approximately follows the outer crater rim and reasonably delineates the almost flat summit plateau (apart from the south sector where sloping flanks start directly above station 3).

3. Data basis and model description

Measurements at AWS3 over the investigation period (IP) 9 February 2005–22 January 2006 (Section 3.1) are used to optimize, run and validate the mass balance model (Section 3.2) which is employed later for sensitivity experiments. The multi-year record from AWS1 is also considered, in order to place the one-year record of AWS3 in a longer temporal context. In addition to the

DOI: 10.1002/joc

continuous measurements, two short-term measurement campaigns were conducted to aid model optimization; they are presented in the model Section 3.2.

3.1. Automated measurements

Continuous measurements at AWS3 comprise the four radiation components (Kipp and Zonen CNR1 net radiometer, mounted horizontally) of incoming and reflected shortwave radiation (wavelength interval: 305–2800 nm) and incoming and outgoing longwave radiation (5000–50 000 nm), air temperature and humidity (Rotronic MP100A) at (initially) 1.05 and 1.75 m height (protected by radiation shields), wind speed and direction (RM Young 05 103–5) at (initially) 1.85 m height, barometric pressure (Setra 278), and surface height change with a sonic ranging sensor (SRS, Campbell SR50) from which the mass turnover at the glacier surface can be deduced (Mölg and Hardy, 2004). The performance of these instruments has been described in association with measurements on glaciers around the world (e.g. Georges and Kaser, 2002; Oerlemans and Klok, 2002; Hardy *et al*., 2003; Klok *et al*., 2005; Van den Broeke *et al*., 2005). Longwave radiation fluxes are also a measure of glacier (radiative) surface temperature, based on the Stefan-Boltzmann law (Van den Broeke *et al*., 2005). Since radiation shields are not artificially ventilated, thermocouples (usually less sensitive to sensor heating) are mounted at the same heights as the Rotronic instruments for reference. All measurements are sampled every 60 s and stored as half-hourly means on a Campbell Scientific CR–23X datalogger. Characteristic measurement errors of the above sensors are described in Van As *et al*. (2005) and Cullen *et al*. (2007b), and their effect on the modelling will be addressed in Section 4.1. Owing to the sub-freezing air temperatures (see below), relative humidity measurements were re-scaled to account for saturation with respect to ice rather than liquid water (*cf* Cullen *et al*., 2007a). Wind speeds (discussed further below as well) are generally high enough to guarantee sufficient (natural) ventilation of the Rotronic sensors (Georges and Kaser, 2002). Nonetheless, we explored the radiation error by comparing 2 °C-binned hourly air temperature data between thermocouple and Rotronic instrument (at initially 1.75 m). Only for the two uppermost bins (-2 to ≤ 0 °C and 0 to ≤ 2 °C) the mean difference is higher than the Rotronic nominal accuracy of 0.3 °C (the Rotronic is higher by 0.7 and 0.9 °C, respectively). Data in these bins ($n = 106$ h) do coincide with high mean hourly global radiation (848 W m^{-2}) and low mean hourly wind speed (1.9 m s^{-1}), which indicates the preconditions for sensor heating are given. However, the issue only concerns 1.27% of the data, so effects neither the mean value of air temperature nor the modelling. Nevertheless we used thermocouple data in this data range as model input (Section 3.2).

Over the IP (348 days), mean air temperature at AWS3 was -6.6 °C, with monthly means varying by less than 1.2 °C around this value. High mean global radiation (incoming shortwave radiation with respect to a horizontal surface) of 340 W m^{-2} (1161 h exceeding 1000 W m^{-2}) and extreme aridity with a mean water vapour pressure of 1.68 hPa and a total precipitation amount of only 1.06 m snow are further characteristics of the high-altitude conditions on Kibo. The net surface mass balance measured with the SRS is -633 mm ice loss, which converts to -570 mm water equivalent (WE) (900 kg m^{-3} for ice density assumed). Figure 2 shows the daily variability of the basic climate variables. Global radiation reflects the annual cycle of the sun, but does not exhibit a minimum around the December solstice. The location of the mountain south of the equator, the near minimum of the sun–earth distance (3 January), and anomalously dry conditions at this time (see below) may explain this fact. Air temperature fluctuates – even on a daily scale – less than ± 3.5 °C around the mean ('thermal homogeneity': Kaser, 2001). Vapour pressure experiences a peak during the MAM wet season, as well as snowfall and snow depth. The absence of a pronounced second peak in these three variables during OND illustrates the failure of the OND snowfall season on Kibo in 2005, which only contributed 11% to the total annual snowfall sum. AWS1, which recorded very similar conditions during the IP, shows this contribution is typically 22% (02/2000–01/2005 mean). Thus, one cause of the negative surface mass balance appears to be the lack of snowfall in the 'short rains' season. Wind speed at AWS3 (Figure 2(d)) did not exhibit a clear annual cycle around its IP mean (5.1 m s^{-1}).

3.2. The mass balance model

Glacier-climate models (e.g. Greuell and Smeets, 2001; Klok and Oerlemans, 2002, 2004) allow computation of the mass balance (MB) of a glacier (or glacier site), which is the sum of accumulation (mass gain) and ablation (mass loss) over a defined time period per unit area (specific MB). While accumulation is reasonably approximated by measured solid precipitation, understanding the ablation component requires the glacier surface energy balance (SEB) and related physical processes to be resolved:

$$S\downarrow(1-\alpha)+L\downarrow+L\uparrow+QS+QL+QG=F \quad (1)$$

Table I (left column) defines the abbreviations used in this equation. Energy fluxes (in W m^{-2}) towards the surface are positive, and negative if directed away from the surface. Mass loss occurs due to sublimation (if QL is negative) and melt. The latter requires the glacier surface temperature (TS) to be at melting point (273.15 K) and the resulting energy flux F to be positive on the right-hand side of Equation (1). If TS is below melting point, F is zero. To solve for F in Equation (1), the MB model first computes (a) in its surface module the glacier-atmosphere energy fluxes from meteorological variables (Table I, right column), and (b) in its subsurface module the vertical temperature distribution inside the

DOI: 10.1002/joc

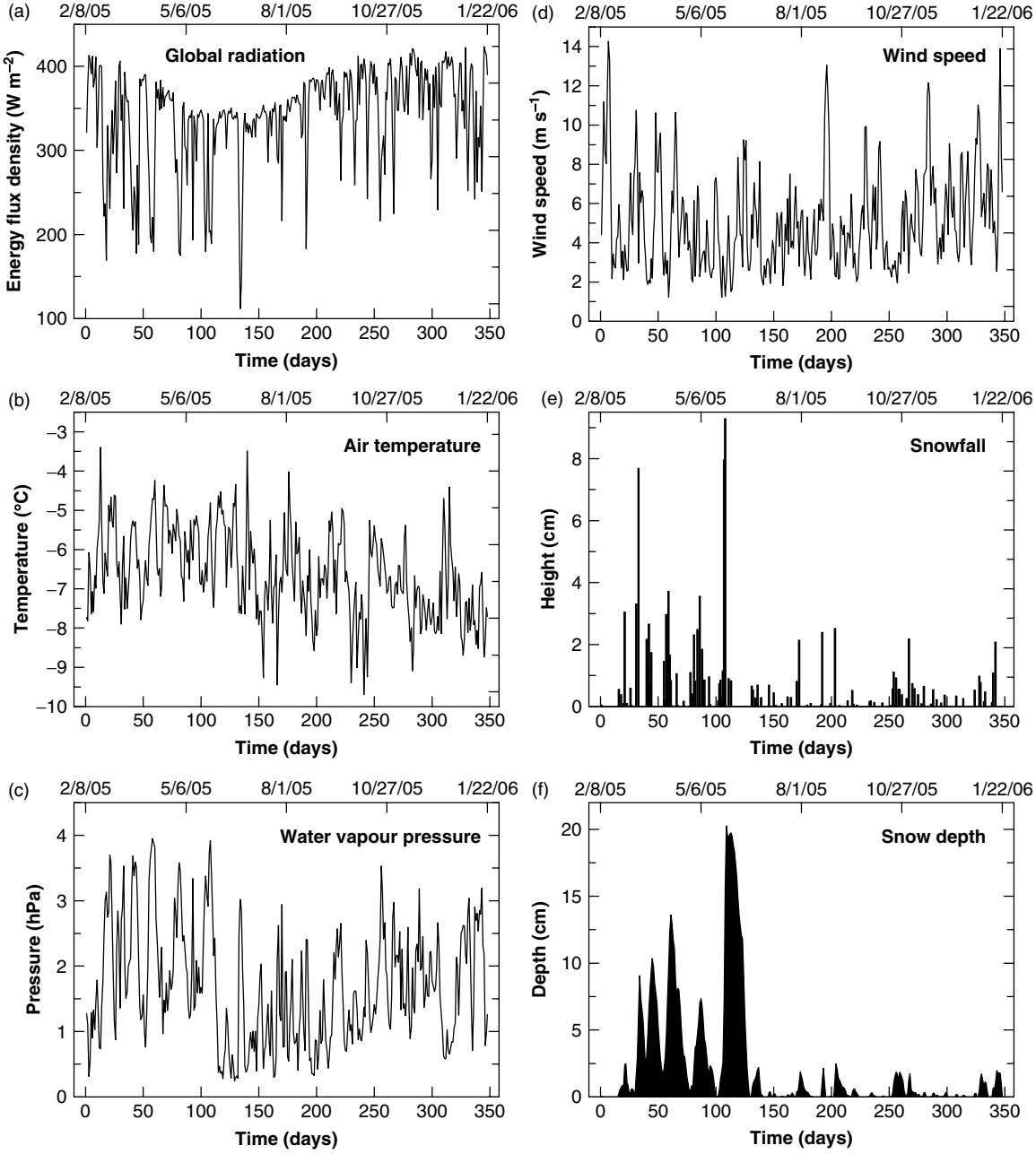

Figure 2. Daily means of (a) global radiation, (b) air temperature, (c) air humidity, and (d) wind speed, and daily (e) accumulation (snowfall) and (f) snow depth (derived from the sonic ranging sensor) at AWS3 between 9 February 2005 (day 1) and 22 January 2006 (day 348). The date (month/day/year) is shown on the upper x-axes.

glacier to solve for *QG*. Secondly, it converts resultant *QL* and *F* to mass fluxes of sublimation and melting from which – together with input of measured accumulation – the surface height change (and thus surface MB) is obtained. The surface and subsurface modules, which are linked through *TS* (Table I, right column), are based on the SEB models of Mölg and Hardy (2004) and Bintanja and Van den Broeke (1995), respectively. The following paragraphs briefly describe relevant details. It should be noted that $S\downarrow$ is the only SEB component in Equation (1) which enters the model as a direct measurement. Other components are parameterized (Table I, right column) in order to perform realistic sensitivity studies, an approach that includes generation of *TS* by the MB model (see further below). We use hourly means from AWS3 to run the model, which results in a total of 8352 time steps over the IP. The sub-daily time steps are required because measured *TS* shows that melting – if it occurs (on 84 of the 348 days) – is limited to a few hours around noon or early afternoon. Mass fluxes can therefore not be captured realistically in daily model steps.

3.2.1. *Net shortwave radiation (S_{NET})*

$S\downarrow$ comes from the direct measurement of global radiation corrected for slope and aspect with a radiation model (Mölg *et al*., 2003a,b). Daily albedo is computed

DOI: 10.1002/joc

Table I. Energy fluxes at the glacier surface and their link to climate as treated in the mass balance model.

Surface energy balance component	Determined from[a]
$S\downarrow$ (incoming shortwave radiation)	Direct measurement of solar radiation
α (surface albedo)	Snowfall amount and frequency, snow depth
$L\downarrow$ (incoming longwave radiation)	Water vapour pressure, air temperature
$L\uparrow$ (outgoing longwave radiation)	Glacier surface temperature (TS)
QS (turbulent sensible heat flux)	Air temperature and TS, wind speed, air pressure
QL (turbulent latent heat flux)	Air humidity and TS, wind speed, air pressure
QG (subsurface energy flux)	Thermodynamic energy equation (forced by TS)

[a] For details see section 3.2.

as a function of snowfall frequency and depth from the albedo model of Oerlemans and Knap (1998) that was developed for year-round conditions on Morteratsch Glacier (Swiss Alps), and introduces five control parameters (CPs): characteristic albedos of fresh snow ($\alpha_{\mathrm{frs}} = 0.75$), of firn ($\alpha_{\mathrm{fi}} = 0.53$) and of ice ($\alpha_{\mathrm{ice}} = 0.34$), an e-folding constant for the effect of ageing on snow albedo ($t^* = 21.9$ days), and an e-folding constant for the effect of snow depth on albedo ($d^* = 3.2$ cm). Our measurements of $S\downarrow$, reflected shortwave radiation, snowfall and snow depth are used to optimize the CPs to Kibo conditions (Figure 3(a)), which goes well for the first half of the IP but does not simulate variability sufficiently during JJAS and OND. Thus, we modified the parameterization and replaced the constant α_{ice} by a variable α_{ice} as a function of dew point temperature (see equation in Figure 3 caption), which increases model performance (Figure 3(b)). Dew point is an important indicator of penitentes that strongly affect albedo (Corripio and Purves, 2005), and these surface features have been observed on Kersten Glacier and at AWS3 during field visits. As ablation on tropical glaciers occurs each day (Kaser, 2001), the term 'firn' is not appropriate for our site, so α_{fi} is called the 'albedo of old snow' (α_{ols}). The optimized, final CPs then read: $\alpha_{\mathrm{frs}} = 0.83$, $\alpha_{\mathrm{ols}} = 0.68$, $t^* = 1.1$ days, and $d^* = 5.1$ cm. The time scale is considerably smaller than on Morteratsch Glacier, indicating that snow is ageing faster on Kibo. This makes sense in view of the year-round ablation on tropical glaciers (Kaser, 2001). The depth scale is slightly larger than on Morteratsch Glacier, indicating that – in case of a snow surface – the albedo of the underlying ice surface impacts the snow albedo more strongly. This seems consistent as well, since snow depths on Kibo are generally low (Figure 2(f)).

3.2.2. *Net longwave radiation (L_{NET})*

$L\downarrow$ is parameterized as a function of air temperature T (in K) and vapour pressure e (in hPa) from a quadratic fit: $L\downarrow = 6854.2904 - 58.0435\ T + 1562.6514\ e + 0.1232\ T^2 - 5.9170\ T\ \ e + 14.9242\ e^2$. The root mean square difference (RMSD) between hourly parameterized and measured $L\downarrow$ is 25.1 W m^{-2} ($r = 0.88$). A more common optimization based on the Stefan–Boltzmann law (e.g. Klok and Oerlemans, 2002; Mölg and Hardy, 2004) does not perform as well (RMSD = 29.5 W m^{-2}, $r = 0.81$) because there is no statistically significant relation between $L\downarrow$ and T in our measurements through a linear fit. On a daily scale, the quadratic fit produces a RMSD of 14.5 W m^{-2} from measurements, which is comparable to other $L\downarrow$ parameterizations (Greuell and Konzelmann, 1994). $L\uparrow$ is obtained conventionally by the Stefan–Boltzmann law from TS and surface emissivity (equal to unity) (Mölg and Hardy, 2004).

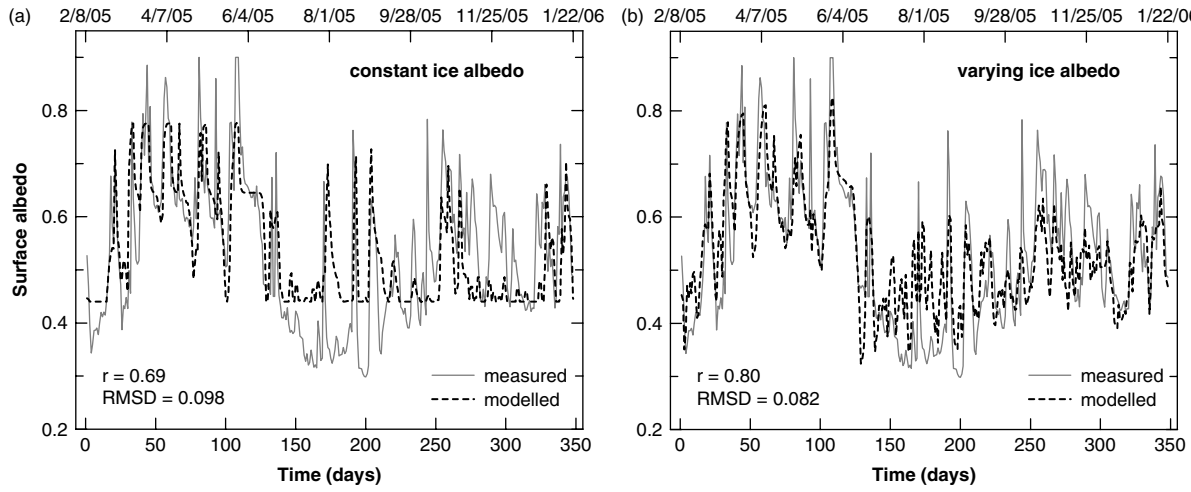

Figure 3. Modelled daily albedo optimized to measurements at AWS3 between 9 February 2005 (day 1) and 22 January 2006 (day 348). (a) Ice albedo as an optimal constant value (0.44), and (b) ice albedo as a varying value, computed as function of daily dewpoint temperature (DPT): $0.0084\,^{\circ}\mathrm{C}^{-1}\ DPT + 0.6487$. Correlation coefficient (r) and root mean square difference (RMSD) are displayed in the lower left corners. The date (month/day/year) is shown on the upper x-axes.

DOI: 10.1002/joc

3.2.3. *Turbulent heat exchange*

QS and *QL* are computed using the 'bulk method' (e.g. Greuell and Smeets, 2001) through analytical expressions (Mölg and Hardy, 2004). Air temperature and humidity from the higher sensor at AWS3 (*cf* Section 3.1) serve as input, because this reduces the relative size of the measurement error (Bintanja and Van den Broeke, 1995). Apart from meteorological input variables (Table I, right column), the 'bulk method' requires a characteristic surface roughness length (SRL) which was explored in an eddy correlation experiment in July 2005 (for logistical reasons at AWS1 which has a roughness element shape similar to AWS3). The experiment (Cullen *et al*., 2007b) suggests SRL = 1.7 mm (for momentum) which, in the model, is also used for scalar SRLs (Mölg and Hardy, 2004; Cullen *et al*., 2007b). Cullen *et al*. (2007b) moreover show that – with the settings described here – the MB model reproduces turbulent heat exchange well compared to direct measurements of *QS* and *QL*.

3.2.4. *Subsurface energy flux*

QG is obtained as the sum of a conductive heat flux (*QC*) and an energy flux from penetrating shortwave radiation (*QPS*). Following Bintanja and Van den Broeke (1995), our subsurface module numerically solves the thermodynamic energy equation (TEE) on a multi-layer grid stretching into the glacier (30 layers, vertical spacing 0.01 m, fixed bottom temperature T_B, see below). The simulated vertical profile of englacial temperature can then be used to determine *QC* from the temperature difference between the surface and the first subsurface layer. If a layer consists of snow and ice, the required values for the thermal diffusivity (1.1 10^{-6} m^2 s^{-1} for ice; 0.4 10^{-6} m^2 s^{-1} for snow), effective thermal conductivity (2.2 W m^{-1} K^{-1} for ice; 0.5 W m^{-1} K^{-1} for snow), and density (900 kg m^{-3} for ice; variable for snow, see below) to solve the TEE and for *QG* are a weighted average (*cf* Klok and Oerlemans, 2002). For the chosen grid spacing, *QPS* is nil and does not impact the subsurface temperature in case of a snow surface, according to Brandt and Warren (1993). In case of an ice surface, a constant fraction $(1 - \zeta)$ S_{NET} penetrates into the subsurface and is attenuated exponentially with depth (Bintanja and Van den Broeke, 1995). Twelve days of subsurface temperature measurements in July 2005 (a period with ice surface) at 0.5 and 2 m depth suggest that (a) *QPS* should be taken into account (otherwise the model produces a cold bias), and (b) the best simulation is reached with $\zeta = 0.71$ (and a constant T_B at 3 m model depth of 269.5 K) (Figure 4). For these optimization runs, the subsurface module was forced with measured *TS*. The optimal ζ is lower than ζ for the Antarctic glacier surface (0.8) used by Bintanja and Van den Broeke (1995), resulting in a higher percentage of S_{NET} penetrating to the glacier subsurface on Kibo. This higher amount for our low-latitude site is in agreement with the theoretical calculations of Warren *et al*. (2002) (*cf* their Figure 6).

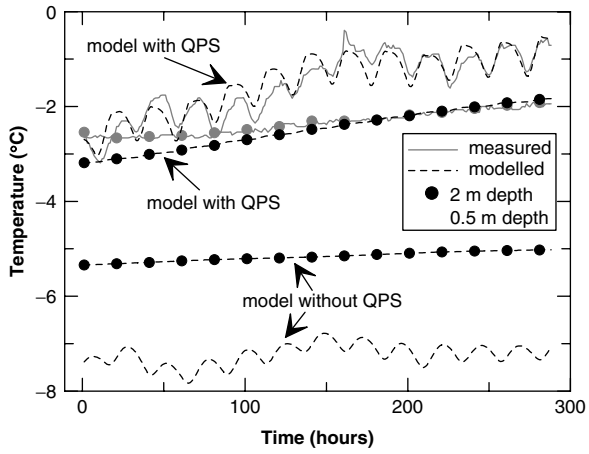

Figure 4. Simulated and measured subsurface temperatures at AWS3 between 31 July 2005 (0100 LT, hour 1) and 11 August 2005 (2400 LT, hour 288) at 0.5 m (lines without point symbols) and 2 m depth (point symbols). Model results are shown with and without activation of penetrating shortwave radiation (QPS).

Extinction coefficients are the same as in Bintanja and Van den Broeke (1995).

3.2.5. *Surface temperature*

TS is a key variable for the SEB (Table I), and additionally links the subsurface and surface modules. It is computed by an iterative procedure (based on bisection interpolation) from the energy availability at the glacier surface under the requirement of equilibrium (ROE) between the SEB fluxes (Mölg and Hardy, 2004). If the resultant *TS* exceeds melting point it is reset to 273.15 K, and the remaining flux *F* represents latent energy flux for melting *QM*. In our preliminary model runs it became clear that – for a realistic simulation of hourly *TS* from the ROE – energy storage in the surface layer must be introduced to Equation (1) (Garratt, 1992).

3.2.6. *Accumulation*

Model surface accumulation is due to measured snowfall rate (model snow density is 285 kg m^{-3}) and *QL*-derived deposition. Model density is consistent with our few measurements of fresh snow density in the field, which was higher than 200 kg m^{-3}. Refreezing of meltwater in the snow pack (internal accumulation) is determined from the temperature and mechanical properties (pore volume, saturation, density) of the snow pack, with the model proposed by Illangasekare *et al*. (1990) coupled to the subsurface module. However, the snow pack is treated as a 'bulk' medium in view of the low snow depths on Kibo (Figure 2(f); Mölg and Hardy, 2004), so the refreezing process is not resolved vertically. In case of refreezing, the latent heat release and related temperature change for the next time step are attributed to the grid points in the snow pack and, again, determined by a weighted-average for the grid point of the subsurface layer that harbours the snow-ice interface. Further, densification of the model snow pack occurs in response to refreezing.

DOI: 10.1002/joc

4. Results and discussion

4.1. Model validation, energy and mass balance

Glacier surface temperature during the IP is shown in Figure 5(a) for the purpose of model validation. There is very good agreement between measurements and model, both in magnitude and interdiurnal variability, which verifies the model's ability to reveal the SEB at AWS3. The typical uncertainty in the $L\uparrow$ measurement of *ca* 10 W m^{-2} (Greuell and Smeets, 2001) leads to a 2.3 K uncertainty in measured *TS* for our data. The RMSD between model and measurement is clearly smaller (Figure 5(a)), and remains smaller on an hourly basis as well (RMSD = 1.2 K). The cold *TS* anomaly (day ~110–135) is linked to the only negative monthly net radiation ($S_{NET} + L_{NET} < 0$; June 2005), as illustrated by the associated glacier-atmosphere energy exchanges in Figure 5(b). All-year negative *QL* indicates continuous mass loss due to sublimation, with a minimum in the MAM wet season when the vapour pressure gradient between surface and overlying air is relatively small. This sublimation pattern strongly resembles the one on the HGS at AWS1 (Mölg and Hardy, 2004). Net shortwave radiation is the main input to, and most varying energy flux on the glacier surface. Its variability is controlled by the surface albedo which therefore represents the key variable in the SEB. Snowfall is the atmospheric variable connected most closely and proportionally to albedo (*cf* Figure 2(e)). Higher and/or more frequent snowfall thus decreases the energy available for ablation. Net longwave radiation shows least negative values in MAM, since the more humid atmosphere in the main wet season (Figure 2(c)) results in highest $L\downarrow$ values. This implies little variability of monthly $L\uparrow$ during the year (less than 11 W m^{-2} around the mean of 278.4 W m^{-2}). The turbulent flux of sensible heat is a small heat gain for the surface and peaks in June 2005. The latter is a cause of the cold *TS* anomaly during this month (Figure 5(a)), which created the largest temperature gradient between surface and overlying air. Still, the slight increase in sensible heat supply in June 2005 could not compensate for the radiative losses (as discussed above) and thus prevent the cold *TS* anomaly.

Turning to the mass fluxes associated with these energy exchanges, Figure 6(a) shows the accumulated glacier surface lowering during the IP, which also serves as the second step in our model validation. Generally there is good agreement between the SRS measurement and the

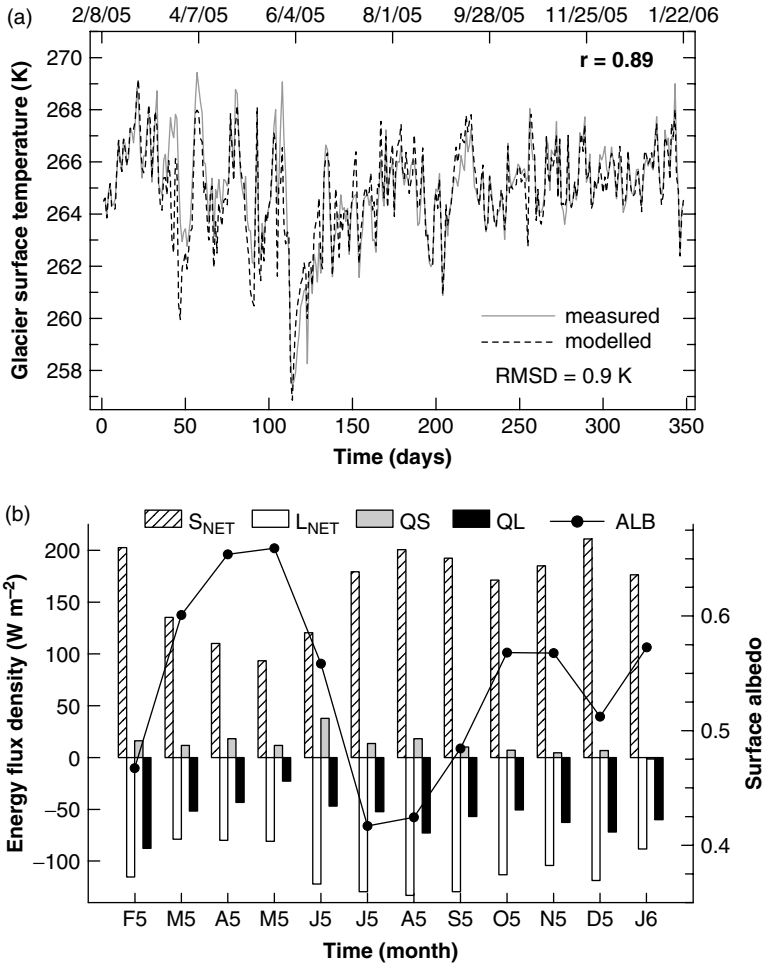

Figure 5. (a) Simulated and measured daily surface temperatures at AWS3 between 9 February 2005 (day 1) and 22 January 2006 (day 348) with correlation coefficient (r) and RMSD displayed. The date (month/day/year) is shown on the upper x-axis. (b) Monthly means of glacier-atmosphere energy fluxes between February 2005 and January 2006. Also shown is surface albedo (line plot, right-hand y-axis).

DOI: 10.1002/joc

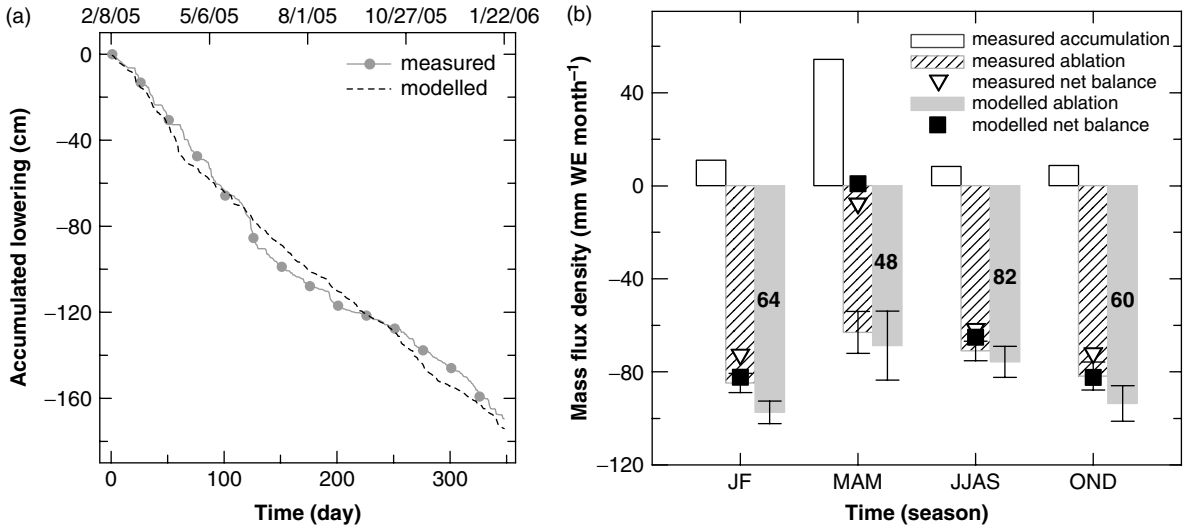

Figure 6. (a) Simulated and measured accumulated surface lowering at AWS3 between 9 February 2005 (day 1) and 22 January 2006 (day 348). The date (month/day/year) is shown on the upper x-axis. (b) Simulated and measured seasonal mass fluxes at the glacier surface for the climatologically wet (MAM, OND) and dry (JF, JJAS) seasons. Bold figures show the modelled contribution of sublimation to mass loss (in %).

model result. The obvious deviation shortly after day 100 could be related to an 'ice bump' that was observed during the July 2005 field visit. This surface element may have disturbed the SRS measurement temporarily, since the SRS record shows unusually large surface changes at this time. Still, the two curves demonstrate continuous ablation throughout the year as it is typical of tropical glaciers (Kaser, 2001); a contrast to the strong seasonality in ablation of extratropical glaciers (e.g. Klok and Oerlemans, 2002).

Figure 6(b) extends the mass flux issue by depicting the seasonal mass balance. For the ablation component, error ranges have been determined for both the measurements and model results. Errors on measured ablation due to the uncertainty in surface height change from the SRS measurement (0.4%) are negligibly small on the seasonal scale (∼1–2 mm WE per season), but exist because of the uncertainty in density of deposited snow. According to field measurements, this density ranges at least between 200 and 300 kg m^{-3} (with values above the upper limit more probable than below the lower limit), so Figure 6(b) is based on 250 ± 50 kg m^{-3} to derive ablation from the SRS. To examine the minimum error on modelled ablation and net mass balance, the MB model has been re-run with offsets in meteorological input variables according to typical instrument errors (8 runs). Following the approach of Greuell and Smeets (2001), we considered 2% uncertainty in measured global radiation and relative humidity, 0.2 °C in air temperature, and 0.2 m s^{-1} in wind speed. Modelled net surface MB over the IP then is -621 ± 95 mm WE, so the measured one (−570 mm WE) is within the uncertainty range. Seasonal mass fluxes are simulated reasonably by the MB model (Figure 6(b)). Owing to the dry conditions, a great part of the total mass loss is due to sublimation (65% on average) as revealed by the model results. This apparently limits the importance of melting and melt water supply. Higher snowfall in the MAM wet season caused (1) a higher albedo and thus less energy available for ablation (as discussed above) and (2) higher accumulation – both of which combined led to the lowest measured net mass loss in the MAM season. Melt water retention in the snowpack accounts for ∼3% in the total MB and ∼6% in the accumulation component, confirming earlier observations that melt water refreezing does occur (Mölg and Hardy, 2004). The simulated maximum snow density due to refreezing is 344 kg m^{-3} and occurs ∼20 days after the peak snow depth in late May (Figure 2(f)). As mentioned above, measured density of deposited snow was occasionally higher than 300 kg m^{-3} (338 and 436 kg m^{-3}), so the model value lies well within the observed range.

Overall, the seasonal mass fluxes (Figure 6(b)) illustrate the failure of snowfall in the OND season in 2005 (*cf* Section 3.1), which shows characteristics very similar to the JF dry season. Table II summarizes energy and mass balance components at AWS3. Despite the good agreement between measurements and model, ablation and surface lowering tend to be higher in the model (Figure 6, Table II). This is because modelled *TS* is more frequently at melting point ($n = 218$ h) than measured *TS* ($n = 177$ h). The amplitude of the diurnal *TS* cycle is therefore slightly greater in the model, given the almost identical values of mean *TS* (Table II). Forcing the MB model with measured *TS* (but maintaining all other settings as described in Section 3.2) reduces modelled surface melt by 59 mm WE, but does not affect sublimation (−5 mm WE) and deposition (−1 mm WE) to any large degree – which brings modelled net surface MB to −568 mm WE. Hence, the difference in net surface MB and surface lowering between measurements and model (as shown in Table II) most probably originates from a melt component that is slightly lower than 341 mm WE.

DOI: 10.1002/joc

Table II. Mass balance components and related variables between 9 February 2005 and 22 January 2006 (total values for the mass balance terms, otherwise averages) from measurements and modelling. NA indicates 'not available'.

Mass balance component or related variable	Modelled	Measured
Incoming shortwave radiation (W m^{-2})	NA	330.6
Surface albedo	0.55	0.54
Incoming (outgoing) longwave radiation (W m^{-2})	170.3 (−278.4)	170.8 (−278.9)
Net radiation (W m^{-2})	44.0	45.4
Turbulent sensible (latent) heat flux (W m^{-2})	13.6 (−55.1)	NA
Total subsurface energy flux (W m^{-2})	0.2	NA
Surface temperature (K)	264.9	265.0
Net surface height change (m)	−0.68	−0.63
Net surface mass balance (mm WE)	-621 ± 95	−570
Surface accumulation (snowfall/deposition), mm WE	306 (303/3)	NA
Internal accumulation (i.e. refreezing), mm WE	19	NA
Surface ablation (melt/sublimation), mm WE	−927 (−341/−586)	NA
Energy for ablation consumed by sublimation (%)	93.6	NA
Bulk snow density (kg m^{-3})	304	NA

4.2. Sensitivity experiments

The sensitivity of a glacier to climate is typically assessed by re-running models with offsets of 20% in precipitation amount (ΔP) and 1 °C in air temperature (ΔT) (e.g. Klok and Oerlemans, 2004). Since snow depth is generated by the MB model (from computed surface lowering), each change of a climate variable leads to a new snow cover evolution, not ΔP solely. Results, based on conditions over the IP, are presented in Figure 7(a) (left). They clearly demonstrate the large impact of ΔP which – on average – is 4.1 times more effective on mass exchange than ΔT. The causal explanation for this response behaviour is that ΔP directly impacts surface albedo, the key variable in the SEB (Section 4.1). The associated 'feedback factor' (FF) defined by Oerlemans and Klok (2004) (ratio of MB change to deposited snow amount change) is 6.4, higher than any FF (*vs* altitude) for a mid-latitude glacier (Oerlemans and Klok, 2004). ΔT affects albedo indirectly through an altered snow cover evolution by changes mainly in the sensible heat flux. However, these changes are small on Kibo compared to albedo-forced changes in net shortwave radiation (*cf* variability of S_{NET} and *QS* in Figure 5(b)). Additionally, ΔP impacts the accumulation component. The implications of precipitation variability are well visible in the IP's MAM season (Figure 6(b)). Higher snowfall increases surface albedo and reduces the main energy source (net shortwave radiation) (*cf* Figure 5(b)), leading to less ablation and – together with higher accumulation – to more balanced mass fluxes (Figure 6(b)). The positive ΔP has a stronger impact than the negative ΔP (Figure 7(a), left), because the change in snow cover hours (compared to the reference run) is greater than in the negative offset scenario (which triggers a stronger albedo feedback).

To investigate whether the predominance of ΔP is maintained at the lower glacier elevations, AWS3 was virtually shifted to 5500 and 5200 m a.s.l. (representative of mid and low elevations of glaciers in the south sector) in Figure 7(b). This was achieved by – as in spatially distributed MB models (Klok and Oerlemans, 2002) – modifying input data with vertical gradients: -0.0055 °C m^{-1} at constant relative humidity for air temperature and humidity, an exponential relation for air pressure (standard barometric formula), and -0.0008 m m^{-1} for snowfall (Røhr and Killingtveit, 2003). An air temperature threshold of 2.5 °C separates snow from rainfall. This value agrees well with a wet bulb temperature of 1 °C (at mean relative humidity on Kibo) suggested by Steinacker (1983). A change in solar radiation was neglected due to the unknown vertical gradient of cloudiness. Reference and sensitivity runs were then repeated for each virtual altitude. Higher air temperature and humidity at lower elevations lead to a more negative net MB in the reference runs (not shown), and seem to decrease but not reverse the difference between ΔP and ΔT effects (Figure 7(b)). The decrease of the ΔP effect at lower altitude may result from the relatively fast degradation of the snow pack under the higher energy availability, which weakens the albedo feedback.

MB sensitivity to climate partly depends on climate conditions of the reference run (not only of the climate zone), and these were somewhat anomalous during the IP ($\Delta P = -18\%$ and $\Delta T = +1$ °C at AWS1 with respect to its February 2000–January 2005 climatology). We thus modified input data to best reconstruct a mean annual cycle for 1979–2004. Monthly anomalies in $S\downarrow$, air temperature, specific humidity, and wind speed for February 2005–January 2006 (with respect to February 1979–January 2005) were computed from NCEP/NCAR reanalysis data (Kalnay *et al*., 1996) for the grid cell covering Kilimanjaro (2.5 °S/37 °E) at 500 hPa (*cf* 502 hPa measured at AWS3). Averaged annual anomalies are (respectively): +1.3 W m^{-2}, +0.44 °C, −0.3 g kg^{-1}, −0.3 m s^{-1} (i.e. $S\downarrow$ and air temperature were higher over the IP than over 1979–2004, humidity and wind speed lower). The hourly AWS3 series for each month (of these four variables) were then multiplied

DOI: 10.1002/joc

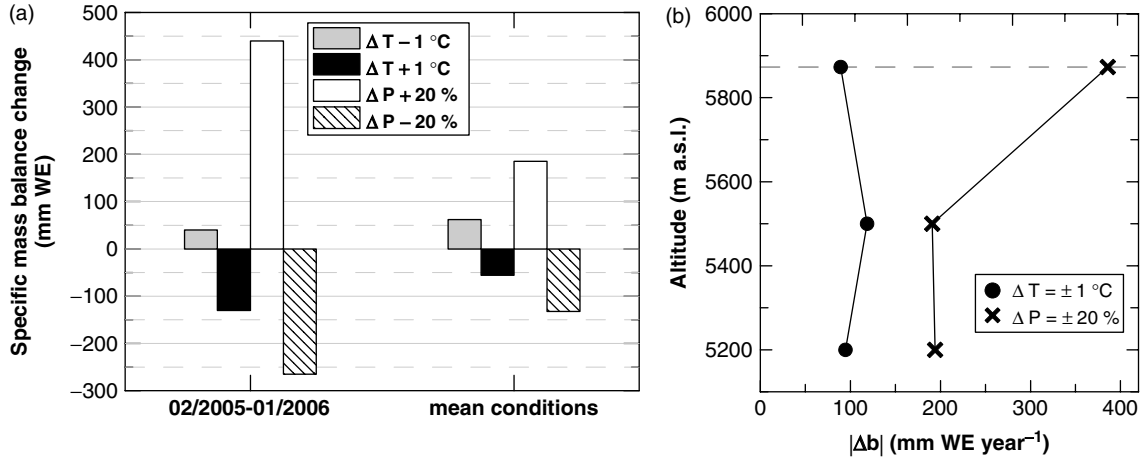

Figure 7. (a) Changes in specific mass balance (with respect to the reference run) at AWS3 due to changes in air temperature (ΔT) and precipitation (snowfall) amount (ΔP) for two reference climates: (left) February 2005 – January 2006 and (right) reconstructed mean conditions over 1979–2004. (b) Change in climate sensitivity with altitude (February 2005 – January 2006 conditions). Displayed mass balance response ($|\Delta b|$) is the absolute change in mass balance averaged from negative and positive offset results (i.e., scenarios that lead to a negative Δb have been counted positive, since signs of Δb remain as in Figure 7(a)). The dashed line indicates the altitude of AWS3 (5873 m a.s.l).

with the corresponding relative monthly NCEP/NACR anomalies (adding absolute anomalies did not change the outcome of the sensitivity runs). This simple approach is supported by the fact that NCEP/NCAR free-air data show skill in reflecting climate anomalies particularly on mountain summits (Hardy *et al.*, 2003; Pepin and Seidel, 2005). Anomalies of snowfall amount (SAM), variability of which is strongly linked to the local scale, were determined with respect to the 5-year (February 2000–January 2005) series at AWS1 (which recorded almost the same SAM over the IP (110 cm) as AWS3 (106 cm)). The highest SAM anomaly in December 2005 (−19.5 cm) is linked to the failure of the 2005 OND snowfall season (*cf* Figure 2(e)). The sensitivity runs were then repeated, this time based on the reference run with modified input data. In principle, this cannot yield as reliable numbers as over the IP (because of the uncertainty involved in the reconstruction), but should at least indicate the direction the sensitivities are shifted. Results show that ranges of ΔT and ΔP sensitivities decrease (Figure 7(a), right), due to the colder atmosphere and presence of OND snowfall in a mean year. Nonetheless, the dominance of ΔP persists (2.7 times more effective than ΔT). The general dominance of ΔP through the related albedo feedback, thus, appears to be a robust result of the sensitivity experiments. A higher snowfall frequency, which is likely to accompany higher precipitation amounts (Hastenrath, 2001; Mölg *et al.*, 2006), would increase the sensitivity to precipitation even further.

Slope glaciers on Kibo are therefore no exception amongst tropical glaciers regarding their sensitivity to climate (*cf* introduction). However, their location far above the mean 0 °C isothermal surface (Figure 2(b)) favours the particularly strong sensitivity to precipitation. Tropical glaciers may show less difference between ΔP and ΔT effects when they are located at lower altitude in the vicinity of the mean 0 °C isothermal surface (e.g. Hastenrath and Kruss, 1992; Favier *et al.*, 2005). In this case air temperature changes affect the phase of precipitation (liquid *vs* solid) and thus the accumulation component of the mass balance too.

4.3. Comparison with other glacier systems on Kibo

The characteristics of SEB, MB and MB sensitivity for the slope glacier (Sections 4.1 and 4.2) show a high similarity to those of the HGS at AWS1, as investigated by Mölg and Hardy (2004). Despite the similarity, keeping HGSs and slope glaciers as separate glacier regimes on Kibo is justified because MB variability on HGSs is not important for areal changes of plateau glaciers as long as the receding vertical ice walls exist at their margins (Cullen *et al.*, 2006). MB variability on slope glaciers, in contrast, does contribute to areal changes without a long delay, considering the fast response time of small slope glaciers in the tropics (Kaser *et al.*, 2003). Further, it appears that HGSs are even more sensitive to precipitation since global radiation (occurring under small solar zenith angles in the tropics) is less attenuated on a horizontal surface compared to a sloping surface – which favours the albedo feedback. In addition (and a focus of future research), incoming and net shortwave radiation probably shows a less complex spatial pattern on the freely-exposed HGSs than on slope glaciers, since the latter's mid and low reaches (i.e. below AWS3) are more heavily influenced by shading and varying slope angles. SEB and MB of the vertical ice walls are governed by solar radiation (Mölg *et al.*, 2003b), but further research is necessary to get insight into turbulent heat exchange on vertical reference surfaces.

5. Conclusions

The presented combination of in-situ measurements with mass balance modelling corroborates that mass fluctuations on Kibo's slope glaciers primarily reflect precipitation variability. The same is true for the horizontal

DOI: 10.1002/joc

surfaces of the plateau glaciers (Mölg and Hardy, 2004). This is a direct cause of the snowfall-albedo feedback that is much stronger than on extratropical glaciers. Glaciers on Kibo are located above the mean freezing level, which keeps absolute magnitude and variability of sensible heat supply small. For this reason, effects of local air temperature changes on mass balance are also small. Results imply that an increase in snowfall would have to be the main climatic requirement to reach long-term net accumulation (mass gain) on horizontal and sloping glacier surfaces and thus prevent formation of the ever-receding vertical ice walls (*cf* Section 2). Other proxy-based studies indeed found that precipitation in East Africa prior to 1880 was substantially higher than in the 20th century ($\sim +20\%$: for a summary see Mölg *et al*., 2006), so our upcoming research will aim to (a) quantify the additional snowfall required to maintain the latest maximum extent of glaciers on Kibo, and (b) assess this result in light of the other proxies. For the present, observed glacier retreat on Kilimanjaro (Cullen *et al*., 2006) (and on Mount Kenya and Rwenzori: Kaser and Osmaston, 2002) most likely reflects drought in the high-elevation zones of East Africa. Since human societies in the tropics mainly depend on precipitation, this provides an important boundary condition for studies of sustainable development issues (e.g. Hay *et al*., 2002; Hemp, 2005). While the retreat of mountain glaciers on a global scale is primarily controlled by rising air temperature (Kaser *et al*., 2006), our results suggest that a regional moisture projection for the 21st century must be incorporated into the framework of a physically-based prediction of glacier retention on Africa's highest mountain. This suggestion is consistent with global warming and regional moisture changes, particularly in the tropics (e.g. Chou *et al*., 2006).

Acknowledgements

This study is funded by the Austrian Science Foundation (FWF, grant no. P17415-N10), the Tyrolean Science Foundation, and the U.S. National Science Foundation (NSF). Local support is provided by the Tanzania Meteorological Agency, and the Commission of Science and Technology (COSTECH). Reanalysis data were provided by the NOAA/OAR/ESRL PSD, Boulder, Colorado, USA, from their Web site (http://www.cdc.noaa.gov/).

References

Bintanja R, Van den Broeke MR. 1995. The surface energy balance of Antarctic snow and blue ice. *Boundary Layer Meteorology* **34**: 902–926.

Brandt RE, Warren SG. 1993. Solar heating rates and temperature profiles in Antarctic snow and ice. *Journal of Glaciology* **39**: 99–110.

Chou C, Neelin JD, Yien-Yi T, Cheng-Ta C. 2006. Regional tropical precipitation change mechanisms in ECHAM4/OPYC3 under global warming. *Journal of Climate* **19**: 4207–4223.

Corripio JG, Purves RS. 2005. Surface energy balance of high altitude glaciers in the Central Andes: the effect of snow penitentes. In *Climate and Hydrology in Mountain Areas*. De Jong C, Collins D, Ranzi R (eds). Wiley and Sons: London; 15–27.

Cullen NJ, Steffen K, Blanken PD. 2007a. Nonstationarity of turbulent heat fluxes at Summit, Greenland. *Boundary-Layer Meteorology* **122**: 439–455, DOI: 10.1007/s10546-006-9112-2.

Cullen NJ, Mölg T, Hardy DR, Steffen K, Kaser G. 2007b. Energy balance model validation on the top of Kilimanjaro using eddy correlation data. *Annals of Glaciology* **46**: (in press).

Cullen NJ, Mölg T, Kaser G, Hussein K, Steffen K, Hardy DR. 2006. Kilimanjaro glaciers: Recent areal extent from satellite data and new interpretation of observed 20th century retreat rates. *Geophysical Research Letters* **33**: L16502, DOI: 10.1029/2006GL027084.

Favier V, Wagnon P, Chazarin JP, Maisincho L, Coudrain A. 2005. One-year measurements of surface heat budget on the ablation zone of Antizana glacier 15, Ecuadorian Andes. *Journal of Geophysical Research* **109**: D18105, DOI: 10.1029/2003JD004359.

Francou B, Vuille M, Wagnon P, Mendoza J, Sicart JE. 2003. Tropical climate change recorded by a glacier in the central Andes during the last decades of the 20th century: Chacaltaya, Bolivia, 16 °S. *Journal of Geophysical Research* **108**: 4059, DOI: 10.129/2002JD002473.

Garratt JR. 1992. *The Atmospheric Boundary Layer*. Cambridge University Press: Cambridge.

Georges C, Kaser G. 2002. Ventilated and unventilated air temperature measurements for glacier-climate studies on a tropical high mountain site. *Journal of Geophysical Research* **107**: 4775, DOI: 10.1029/2002JD002503.

Greuell W, Konzelmann T. 1994. Numerical modeling of the energy balance and the englacial temperature of the Greenland Ice sheet, calculation for the ETH-Camp location (West Greenland, 1155 m asl). *Global and Planetary Change* **9**: 91–114.

Greuell W, Smeets P. 2001. Variations with elevation in the surface energy balance on the Pasterze (Austria). *Journal of Geophysical Research* **106**: 31,717–31,727.

Hardy DR, Vuille M, Bradley RS. 2003. Variability of snow accumulation and isotopic composition on Nevado Sajama, Bolivia. *Journal of Geophysical Research* **108**: 4693, DOI: 10.1029/2003JD003623.

Hastenrath S. 2001. Variations of East African climate during the past two centuries. *Climatic Change* **50**: 209–217.

Hastenrath S, Kruss PD. 1992. The dramatic retreat of mount Kenya's glaciers between 1963 and 1987: greenhouse forcing. *Annals of Glaciology* **16**: 127–133.

Hay SI, Cox J, Rogers DJ, Randolphs SE, Stern DI, Shanks GD, Myers MF, Snow RW. 2002. Climate change and the resurgence of malaria in the East African highlands. *Nature* **415**: 905–909.

Hemp A. 2005. Climate change driven forest fires marginalize the impact of ice cap wasting on Kilimanjaro. *Global Change Biology* **11**: 1013–1023, DOI: 10.111/j.1365–2486.2005.00968.x.

Illangasekare TH, Rodney JW Jr, Meier MF, Pfeffer WT. 1990. Modeling of meltwater infiltration in subfreezing snow. *Water Resources Research* **26**: 1001–1012.

Kalnay E, Kanamitsu M, Kistler R, Collins W, Deaven D, Gandin L, Iredell M, Saha S, White G, Woollen J, Zhu Y, Leetmaa A, Reynolds B, Chelliah M, Ebisuzaki W, Higgins W, Janowiak J, Mo KC, Ropelewski C, Wang J, Jenne R, Joseph D. 1996. The NCEP/NCAR 40-year reanalysis project. *Bulletin of the American Meteorological Society* **77**: 437–471.

Kaser G. 2001. Glacier-climate interactions at low latitudes. *Journal of Glaciology* **47**: 195–204.

Kaser G, Georges C. 1997. Changes in the equilibrium line altitude in the tropical cordillera Blanca (Perú) between 1930 and 1950 and their spatial variations. *Annals of Glaciology* **24**: 344–349.

Kaser G, Osmaston H. 2002. *Tropical Glaciers*. Cambridge University Press: Cambridge.

Kaser G, Juen I, Georges C, Gomez J, Tamayo W. 2003. The impact of glaciers on the runoff and the reconstruction of mass balance history from hydrological data in the tropical Cordillera Blanca, Perú. *Journal of Hydrology* **282**: 130–144.

Kaser G, Hardy DR, Mölg T, Bradley RS, Hyera TM. 2004. Modern glacier retreat on Kilimanjaro as evidence of climate change: Observations and facts. *International Journal of Climatology* **24**: 329–339.

Kaser G, Cogley JG, Dyurgerov MB, Meier MF, Ohmura A. 2006. Mass balance of glaciers and ice caps: Consensus estimates for 1961–2004. *Geophysical Research Letters* **33**: L19501, DOI: 10.1029/2006GL027511.

Klok EJ, Oerlemans J. 2002. Model study of the spatial distribution of the energy and mass balance of Morteratschgletscher, Switzerland. *Journal of Glaciology* **48**: 505–518.

Klok EJ, Oerlemans J. 2004. Modeled climate sensitivity of the mass balance of Morteratschgletscher and its dependence on albedo parameterization. *International Journal of Climatology* **24**: 231–245.

Klok EJ, Nolan M, Van den Broeke MR. 2005. Analysis of meteorological data and the surface energy balance of McCall Glacier, Alaska, USA. *Journal of Glaciology* **51**: 451–461.

Kruss PD, Hastenrath S. 1987. The role of radiation geometry in the climate response of mount Kenya's glaciers, part 1: horizontal reference surfaces. *International Journal of Climatology* **7**: 493–505.

Mölg T, Hardy DR. 2004. Ablation and associated energy balance of a horizontal glacier surface on Kilimanjaro. *Journal of Geophysical Research* **109**: D16104, DOI: 10.1029/2003JD004338.

Mölg T, Georges C, Kaser G. 2003a. The contribution of increased incoming shortwave radiation to the retreat of the Rwenzori Glaciers, East Africa, during the 20th century. *International Journal of Climatology* **23**: 291–303.

Mölg T, Hardy DR, Kaser G. 2003b. Solar-radiation-maintained glacier recession on Kilimanjaro drawn from combined ice-radiation geometry modeling. *Journal of Geophysical Research* **108**: 4731, DOI: 10.1029/2003JD003546.

Mölg T, Renold M, Vuille M, Cullen NJ, Stocker TF, Kaser G. 2006. Indian ocean zonal mode activity in a multicentury-integration of a coupled AOGCM consistent with climate proxy data. *Geophysical Research Letters* **33**: L18710, DOI: 10.1029/2006GL026384.

Oerlemans J, Knap WH. 1998. A 1 year record of global radiation and albedo in the ablation zone of Morteratschgletscher, Switzerland. *Journal of Glaciology* **44**: 231–238.

Oerlemans J, Klok EJ. 2002. Energy balance of a glacier surface: Analysis of automatic weather station data from the Morteratschgletscher, Switzerland. *Arctic, Antarctic, and Alpine Research* **34**: 477–485.

Oerlemans J, Klok EJ. 2004. Effect of summer snowfall on glacier mass balance. *Annals of Glaciology* **38**: 97–100.

Osmaston H. 1989. Glaciers, glaciations and equilibrium line altitudes on Kilimanjaro. *Quarternary and Environmental Research on East African Mountains*, Mahaney WC (ed). Balkema: Rotterdam; 7–30.

Pepin NC, Seidel DJ. 2005. A global comparison of surface and free-air temperatures at high elevations. *Journal of Geophysical Research* **110**: D03104, DOI: 10.1029/2004JD005047.

Rodhe H, Virji H. 1976. Trends and periodicities in East African rainfall. *Monthly Weather Review* **104**: 307–315.

Røhr PC, Killingtveit AA. 2003. Rainfall distribution on the slopes of Mt. Kilimanjaro. *Hydrological Science-Journal-des Sciences Hydrologiques* **48**: 65–78.

Steinacker R. 1983. Diagnose und Prognose der Schneefallgrenze. *Wetter und Leben* **35**: 81–90.

Thompson LG, Mosley-Thompson E, Davis ME, Henderson KA, Brecher HH, Zagorodnov VS, Mashiotta TA, Lin P, Mikhalenko VN, Hardy DR, Beer J. 2002. Kilimanjaro ice core records: Evidence of Holocene climate change in tropical Africa. *Science* **298**: 589–593.

Van As D, Van den Broeke MR, Reijmer C, Van de Wal R. 2005. The summer surface energy balance of the high Antarctic plateau. *Boundary-Layer Meteorology* **115**: 289–317.

Van den Broeke MR, Van As D, Reijmer C, Van de Wal R. 2005. Sensible heat exchange at the Antarctic snow surface: A study with automatic weather stations. *International Journal of Climatology* **25**: 1081–1101.

Wagnon P, Ribstein P, Francou B, Sicart JE. 2001. Anomalous heat and mass budget of Glaciar Zongo, Bolivia, during the 1997/98 El Niño year. *Journal of Glaciology* **47**: 21–28.

Warren SG, Brandt RE, Grenfell TC, McKay CP. 2002. Snowball earth: Ice thickness on the tropical ocean. *Journal of Geophysical Research* **107**: 3167, DOI: 10.1029/2001JC001123.